Applied Mathematics and Computation 266 (2015) 316–327

Contents lists available at ScienceDirect

Applied Mathematics and Computation

journal homepage: www.elsevier.com/locate/amc

# High-order finite volume shallow water model on the cubed-sphere: 1D reconstruction scheme

Kiran K. Katta[a,b], Ramachandran D. Nair[b], Vinod Kumar[a,*]

[a] The University of Texas at El Paso, El Paso, TX 79902, USA
[b] National Center for Atmospheric Research, Boulder, CO 80305, USA

ARTICLE INFO

*Keywords:*
High order scheme
Shallow water equations
Cubed-sphere grid
Advection-diffusion
WENO
Climate modeling

ABSTRACT

A central-upwind finite-volume (CUFV) scheme for shallow-water model on a nonorthogonal equiangular cubed-sphere grid is developed, consequently extending the 1D reconstruction CUFV transport scheme developed by us. High-order spatial discretization based on weighted essentially non-oscillatory (WENO) is considered for this effort. The CUFV method combines the alluring features of classical upwind and central schemes. This approach is particularly useful for complex computational domain such as the cubed-sphere. The continuous flux-form spherical shallow water equations in nonorthogonal curvilinear coordinates are utilized. Fluxes along the element boundaries are approximated by a Kurganov–Noelle–Petrova scheme. A fourth-order strong stability preserving Runge–Kutta time stepping scheme for time integration is employed in the present work. The numerical scheme is evaluated with standard shallow water test suite, which accentuate accuracy and conservation properties. In addition, an efficient yet inexpensive bound preserving filter with an optional positivity filter is used to remove spurious oscillations and to achieve strictly positive definite numerical solution. To tackle the discontinuities that arise at the edges of the cubed-sphere grid, we utilize a high-order 1D interpolation procedure combining cubic and quadratic interpolations.The results with the high-order scheme is compared with the results for the same tests for various schemes available in literature. Since, the scheme presented here uses local-cell information, it is expected to be scalable to high number of processors count in a distributed node high-performance computer.



## 1. Introduction

Finite-volume (FV) methods offer many computationally desirable properties including inherent conservation, ease of applying monotonicity (non-oscillatory, positivity-preserving properties etc.), geometric flexibility to adapt to complex grid systems and have the potential to utilize available massive parallel computers. Because of these features FV based discretization techniques are becoming increasingly popular in atmospheric numerical modeling. In addition, the new generation atmospheric (climate) models are computationally intense and are designed for currently available petascale computers. For parallel efficiency of the model, the choice of underlying numerical algorithm and spherical grid system (computational domain) are very crucial and directly linked to the scalability of the model. For example, the new generation atmospheric models avoid using the global spectral transform methods due to its *non-local* nature which impedes efficient parallel implementation. However, FV

* Corresponding author. Tel.: +9157476075.
*E-mail address:* vkumar@utep.edu, vk.rice@gmail.com (V. Kumar).

http://dx.doi.org/10.1016/j.amc.2015.04.053
0096-3003/

scheme being *local* method is a very good choice for spatial discretization. The disadvantage of these CUFV schemes is that they are more diffusive than analogous discretizations which use expensive and complicated approximate Riemann solvers. Although element-based Galerkin schemes such as the high-order continuous and discontinuous Galerkin methods provide excellent parallel scalability ([1–4]), they have stringent Courant–Friedrichs–Lewy (CFL) stability limit with explicit time-stepping, and issues with creating a non-oscillatory solution ([5–7]).

Representation of the spherical geometry plays a vital role in the performance of the modern FV based model. Latitude-longitude grid system is a popular choice but has a stringent limitation to scale to massively parallel machines, and also has complications close to the poles, due to the singularities in the governing equations, these reasons make latitude-longitude grid systems not favorable for the next generation global modeling systems. Other choices for global grid systems are the icosahedral hexagonal grid [8–10], Yin–Yang grid [11] and cubed-sphere grid [12,13], these grid systems provide quasi-uniform grid structures (control-volumes). Cubed-sphere grid is gaining popularity, since it is free from polar singularities, and its grid uniformity leads to excellent parallel efficiency [14,15]. The cubed-sphere grid system is very well suited for FV discretization, because of the underlying control volumes (grid cells) are logically rectangular, facilitating easy implementation. Cubed-sphere consists of six identical spherical patched surfaces, which are discontinuous at the edges and corners. These edges and corners need preferential treatment. In order to predict the cell-averages at the new time level, FV methods require a reconstruction procedure for fluxes at the cell edges from the known cell-averages. This involves a computational halo region (stencil) encompassing several grid cells. We make use of high-order 1D interpolation procedure combining cubic and quadratic interpolations for calculation of cell averages in the halo region.

In modeling of the global atmospheric flows, the shallow water equations on sphere are considered to be the standard test problems. Spherical shallow-water models are often used as a test-bed to validate horizontal aspects of the numerical schemes of a complex 3D model. Williamson et al. [16] standardized a suite of tests for global shallow water models. Recently, several upwind-based FV numerical schemes have been tested in shallow-water models on the cubed-sphere [15,17–19]. However, these models employ specialized Riemann solvers which are computationally cumbersome, particularly for the nonorthogonal curvilinear geometry. In this present work we employ the cubed-sphere grid for the proposed FV scheme, and validate the performance by using benchmark tests [16].

High-order extensions of Godunov schemes are the basis of presently available large class of FV methods for solving hyperbolic conservation laws, collectively known as the Godunov-type schemes [20,21]. These schemes essentially have three basic steps in the solution process: reconstruction, evolution and projection. They are broadly classified into upwind and central schemes depending on the final projection step. Upwind schemes employ Riemann solvers to resolve discontinuity at cell interfaces, this requires characteristic information of the wave propagation at the discontinuity (Riemann fans), often resulting in a complex and expensive upwind algorithm (see for example [15,17,22]). Where as the central schemes do not require characteristic decomposition or expensive Riemann solvers, and the projection is done by averaging over the Riemann fans [23], nevertheless, the central schemes are dissipative but computationally inexpensive. The central-upwind finite-volume (CUFV) scheme combines the nice features of the classical upwind and central FV methods as introduced in [24–28]. Semi-discrete formulation of CUFV schemes avoid staggered grids and are relatively easy to implement for practical applications, moreover, due to the semi-discretized formulation time integration can be performed by explicit high-order Runge–Kutta method.

The spatial order of accuracy as well as non-oscillatory property of central FV scheme depends on the reconstruction polynomials. The high-order weighted essentially non-oscillatory (WENO) method ([29]) can be utilized in the reconstruction stage as shown in [26]. The WENO philosophy of Jiang and Shu [30] involves a weighted sum of polynomials where the least oscillatory polynomials are weighted the highest, which results in a class of robust reconstruction procedure. Recently, Katta et al. [31,32] tested two CUFV schemes on cubed-sphere for a transport problem with strict monotonicity option. The reconstruction in the present work relys on a fifth-order WENO (WENO-5), a dimension-split 1D reconstruction. In the present work, we extend the CUFV transport scheme [32] further by solving shallow-water equations on the cubed-sphere.

The remainder of the paper is organized as follows. Section 2 describes the shallow water formulation on the cubed-sphere. Section 3 introduces CUFV scheme with WENO-5 reconstruction. Numerical experiments are given in Section 4, followed by results and conclusions in Section 5.

## 2. Shallow water model

In this work, the cubed-sphere geometry and the continuous flux form non-linear shallow water (SW) equations in curvilinear coordinates are considered to test the performance of the proposed CUFV scheme.

### 2.1. Cubed-sphere geometry

The cubed-sphere geometry was introduced by Sadourny [12], which became popular in atmospheric modeling community [13,33]. The cubed-sphere geometry consists of partitioning sphere $\mathcal{S}$ into six identical regions which are obtained by the equiangular central projection (gnomonic) projection of the faces of the inscribed cube onto the surface of $\mathcal{S}$. Each of the local coordinate systems is free of singularities, and creates a nonorthogonal curvilinear coordinate system on $\mathcal{S}$. The cubed-sphere grid provides a quasi-uniform rectangular grid (logically rectangular) on the sphere without pole problems. This type of grid system has been recently adapted by a number of cell-centered FV methods (see [14,17,18,31,34]) Cubed-sphere grid system

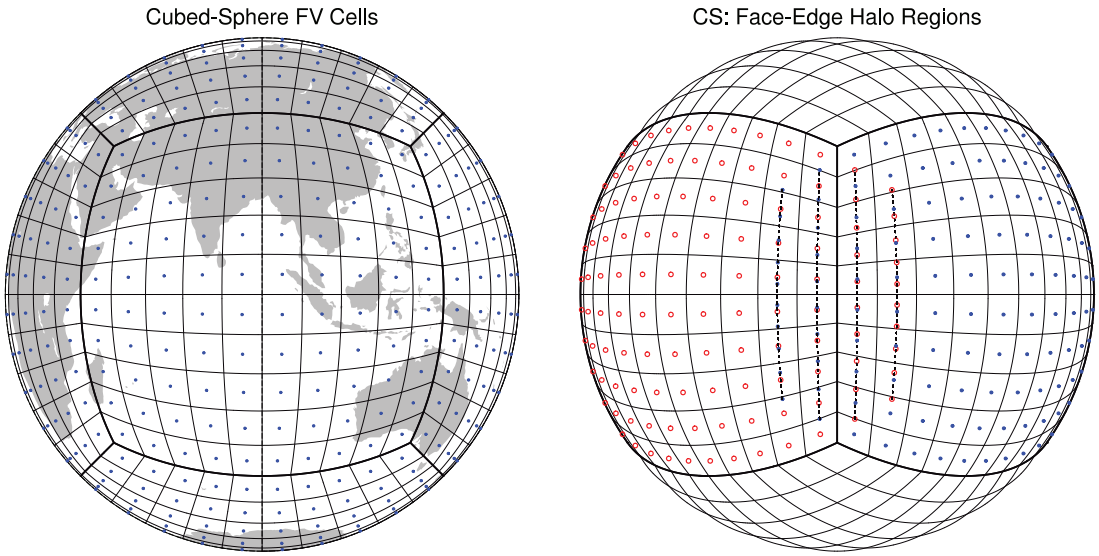


**Fig. 1.** Schematic (left) of a cubed-sphere with cell-centered points for each cell. Each face of the cubed-sphere is partitioned into $N_c \times N_c$ cells (control volumes) for the FV discretization, $6N_c^2$ cells span the entire spherical surface. The right panel shows a cubed-sphere edge with two cell-wide extension to create halo regions. The grid-lines along $x^1$-direction extended at the edges by performing 1D interpolation in $x^2$-direction (shown as dotted arcs) over the halo zone, which lies on the neighboring face.

is highly scalable on currently available massively parallel computer architectures. There are different variants for the cubed-sphere grid system, however, here we consider the cubed-sphere geometry employing the equiangular central (gnomonic) projection.

A sphere $\mathcal{S}$ with radius $R_a$ is decomposed into six identical regions, by an equiangular central (gnomonic) projection of the faces of an inscribed cube. The central angles of projection $x^1 = x^1(\lambda, \theta)$, $x^2 = x^2(\lambda, \theta)$ are the local coordinates for each face such that $x^1, x^2 \in [-\pi/4, \pi/4]$, where $\lambda$ and $\theta$, are respectively, the longitude and the latitude of the sphere $\mathcal{S}$. This results in a nonorthogonal curvilinear coordinate system $(x^1, x^2)$, which is free of singularities. Fig. 1 shows a cubed-sphere with $N_c \times N_c$ cells (control volumes) on each face. The orientation of the different cube faces and their local connectivity is shown in [35].

The metric tensor associated with the central projection is given by:

$$G_{\imath\jmath} = \frac{R_a^2}{\rho^4 \cos^2 x^1 \cos^2 x^2} \times \begin{bmatrix} 1+\tan^2 x^1 & -\tan x^1 \tan x^2 \\ -\tan x^1 \tan x^2 & 1+\tan^2 x^2 \end{bmatrix} \tag{1}$$

where $\rho^2 = 1 + \tan^2 x^1 + \tan^2 x^2$, and the tensor indices $\imath, \jmath \in \{1, 2\}$. The Jacobian (metric term) of the transformation is $G = \det[G_{\imath\jmath}]$. The horizontal velocity vector on the sphere $\mathbf{v}(\lambda, \theta) = (u_s, v_s)$ can be expressed in terms of covariant $(u_1, u_2)$ and contravariant $(u^1, u^2)$ vectors, which are related through the tensor relation $u_\imath = G_{\imath\jmath} u^\jmath$, $u^\imath = G^{\imath\jmath} u_\jmath$ where $G^{\imath\jmath} = G_{\imath\jmath}^{-1}$. For each face of the cubed-sphere,

$$\begin{bmatrix} u^1 \\ u^2 \end{bmatrix} = \mathbf{A}^{-1} \begin{bmatrix} u_s \\ v_s \end{bmatrix}, \quad \begin{bmatrix} u_1 \\ u_2 \end{bmatrix} = \mathbf{A}^{\mathbf{T}} \begin{bmatrix} u_s \\ v_s \end{bmatrix} \tag{2}$$

where

$$\mathbf{A} = R_a \begin{bmatrix} \cos\theta(\partial\lambda/\partial x^1) & \cos\theta(\partial\lambda/\partial x^2) \\ \partial\theta/\partial x^1 & \partial\theta/\partial x^2 \end{bmatrix}. \tag{3}$$

The matrix $\mathbf{A}$ is local to each face of the cubed-sphere such that $G_{\imath\jmath} = \mathbf{A}^{\mathbf{T}}\mathbf{A}$. For the details of the local transformation laws and the matrix $\mathbf{A}$ see [35].

### 2.2. Shallow water equations

Flux-form shallow water equations in curvilinear coordinates are considered in this present work, which is equivalent to the vector-invariant form [36]. The shallow water equations are derived from depth-integrating the Navier–Stokes equations, the horizontal length scale is considered to be much greater than the vertical length scale. Under this condition, conservation of mass implies that the vertical velocity of the fluid is insignificant and can be neglected.

The governing equations for an inviscid flow of a thin layer of fluid in two-dimension (2D) are the horizontal momentum and continuity equations for the height $h$, where $h$ is the height of the fluid and is related to free surface geo-potential height (above sea level) $\Phi = g(h_s + h)$, here $h_s$ is the height of underlying mountains and gravitational acceleration is denoted by $g$.

The continuity and momentum equations for the shallow water system in curvilinear coordinates, can be represented as follows ([3,13]):

$$\frac{\partial}{\partial t}(\sqrt{G}h) + \frac{\partial}{\partial x^1}(\sqrt{G}u^1 h) + \frac{\partial}{\partial x^2}(\sqrt{G}u^2 h) = 0, \tag{4}$$

$$\frac{\partial u_1}{\partial t} + \frac{\partial}{\partial x^1}(E) = -\sqrt{G}u^2(f+\zeta), \tag{5}$$

$$\frac{\partial u_2}{\partial t} + \frac{\partial}{\partial x^2}(E) = \sqrt{G}u^1(f+\zeta), \tag{6}$$

Where

$$E = \Phi + \frac{1}{2}(u_1u^1 + u_2u^2), \qquad \zeta = \frac{1}{\sqrt{G}}\left[\frac{\partial u_2}{\partial x^1} - \frac{\partial u_1}{\partial x^2}\right], \quad f = 2\omega\sin\theta$$

Here $f$ is the Coriolis parameter, $\omega$ is the rotation rate of the earth and $\zeta$ is the relative vorticity.

The six local cartesian coordinate systems $(x^1, x^2)$ are projected onto the sphere using equi-angular central projection [3], in such a way that $x^1 = x^1(\lambda, \theta)$, $x^2 = x^2(\lambda, \theta)$, and $-\frac{\pi}{4} \le x^1, x^2 \le \frac{\pi}{4}$. The flux form of the shallow water equations (4)–(6) can be written as:

$$\frac{\partial}{\partial t}(\mathbf{U}) + \frac{\partial}{\partial x^1}\mathbf{F_1}(U) + \frac{\partial}{\partial x^2}\mathbf{F_2}(U) = \mathbf{S}(U) \tag{7}$$

Where $\mathbf{U} = [\sqrt{G}h, u_1, u_2]^T$, $\mathbf{F_1} = [\sqrt{G}hu^1, E, 0]^T$, $\mathbf{F_2} = [\sqrt{G}hu^2, 0, E]^T$ and source term $\mathbf{S} = [0, \sqrt{G}u^2(f+\zeta), -\sqrt{G}u^1(f+\zeta)]^T$.

## 3. CUFV scheme for cubed-sphere geometry

For simplicity, we consider a scalar component of Eq. (7) to describe descretization. The flux form Eq. (7) can be represented as follows:

$$\frac{\partial U}{\partial t} + \nabla \cdot \mathbf{F}(U) = S(U), \quad \text{in } D \times (0, T), \tag{8}$$

for all $(x^1, x^2) \in D$, and initial condition $U_0(x^1, x^2) = U(x^1, x^2, t = 0)$. In Eq. (8), $U = U(x^1, x^2, t)$, gradient operator $\nabla = (\partial/\partial x^1, \partial/\partial x^2)$, $\mathbf{F} = (F_1, F_2)$ is the flux function, and $S(U)$ is the source term. $D$ is the computational domain, spanning six identical non-overlapping sub-domains of the surface of cubed-sphere, herein, we only define descretization for single subdomain $\Omega$, since all the faces of cubed-sphere are identical.

The subdomain $\Omega$ is partitioned into $N_c \times N_c$ non-overlapping rectangular cells $\Omega_{i,j}$, where $i, j = 1,2,...,N_c$, so that $\Omega_{ij} = [(x^1 \in (x^1_{i-1/2}, x^1_{i+1/2}), x^2 \in (x^2_{j-1/2}, x^2_{j+1/2})]$. The total number of cells on the cubed-sphere are $M = 6 \times N_c \times N_c$. The size of each cell is $x^1_i = (x^1_{i+1/2} - x^1_{i-1/2})$ and $x^2_i = (x^2_{j+1/2} - x^2_{j-1/2})$ in $x^1$ and $x^2$ directions respectively.

The semi-discrete CUFV scheme corresponding to (8) can be represented as follows [32]:

$$\frac{\partial \overline{U}_{ij}}{\partial t} = \frac{-1}{\Delta x^1_i \, \Delta x^2_j}\left[\sum_{k=1}^{4}\int_{\gamma_k} \hat{\mathbf{F}} \cdot \mathbf{n}\right] + \overline{S}_{ij}, \tag{9}$$

where $\overline{U}_{ij}$ is the cell-average, $\hat{\mathbf{F}}$ is the numerical flux function defined at the cell walls (interfaces), and $\overline{S}_{ij}$ is the cell-averaged source term. The line integrals along the cell walls are evaluated using three-point Simpson's rule, as indicated on the right panel of Fig. 2. Here we only show the evaluation for the east wall, and the evaluation for the other walls follows the same pattern. The formula is given as:

$$\int_{\gamma_{East}} \hat{\mathbf{F}} \cdot \mathbf{n} \approx \frac{\Delta x^2_j}{6}\left[H_{i+1/2,j-1/2} + 4H_{i+1/2,j} + H_{i+1/2,j+1/2}\right], \tag{10}$$

where $H_{i+1/2,j}$ is the one-sided central-upwind flux formula [25], which is dependent on the local speed $a_{i+1/2,j}$ as follows:

$$H_{i+1/2,j} = \frac{a^+_{i+1/2,j}F(U^-_{i+1/2,j}) - a^-_{i+1/2,j}F(U^-_{i+1/2})}{a^+_{i+1/2,j} - a^-_{i+1/2,j}} + \frac{a^+_{i+1/2,j}a^-_{i+1/2,j}}{a^+_{i+1/2,j} - a^-_{i+1/2,j}}\left[U^+_{i+1/2,j} - U^-_{i+1/2,j}\right]. \tag{11}$$

where $a^+$ and $a^-$ are local speeds which are given by the eigenvalues $\lambda_1 < \lambda_2 < \cdots < \lambda_N$ of the flux Jacobian ( $\partial\mathbf{F}/\partial U$) at the left ($U^-$) and the right ($U^+$) sides of the cell interface, and defined to be [25,37]:

$$a^+ = \max\left\{\lambda_N\left(\frac{\partial \mathbf{F}}{\partial U}\right), 0\right\}, \quad a^- = \left|\min\left\{\lambda_1\left(\frac{\partial \mathbf{F}}{\partial U}\right), 0\right\}\right|.$$

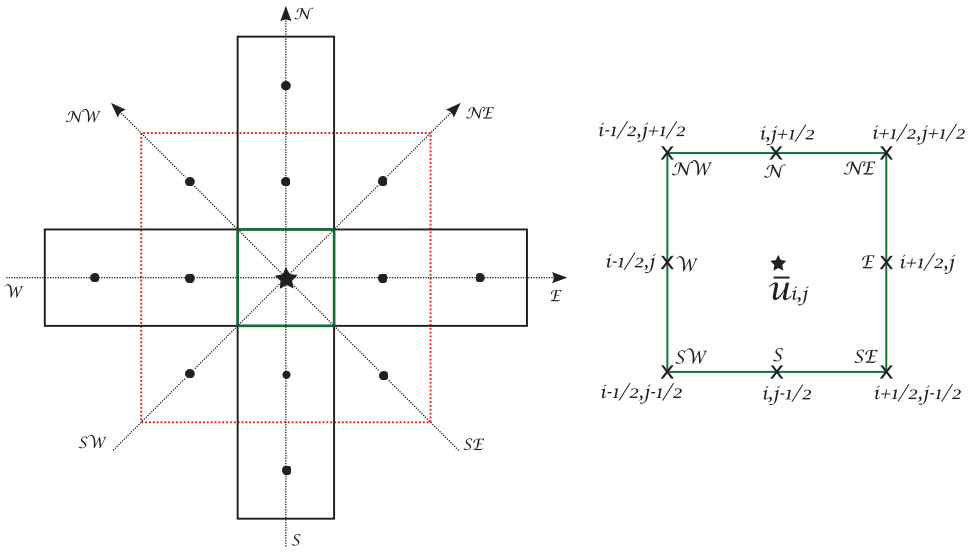


**Fig. 2.** 2D stencil (left) for KL scheme. Thick lines indicate the 2D stencil (W-E and S-N direction) for WENO-5 scheme. Schematic of a 2D control volume (right), where the fluxes are evaluated on the cell boundaries at eight points ('X' marks). Non-oscillatory reconstruction polynomials are used for the flux evaluation.

For the SW equations on cubed-sphere geometry, the eigenvalues of the flux Jacobian are given in [3]. In $x^1$-direction eigenvalues are $\{u^1, u^1 \pm \sqrt{\Phi G^{11}}\}$, similarly in $x^2$-direction they are $\{u^2, u^2 \pm \sqrt{\Phi G^{22}}\}$.

To evaluate the flux $H_{i+1/2,j}$ in Eq. (11), eight point-values along the cell walls (as shown in Fig. 2) are required. These values are computed from 2D piecewise reconstruction polynomials $P_{ij}^n(x^1, x^2) \approx U_{ij}^n(x^1, x^2)$ at time $t = t^n$, where $U_{ij}^n(x^1, x^2) = U(x^1, x^2, t^n)|_{\Omega_{ij}}$. Reconstruction polynomials are subject to the following conservation constraint,

$$\overline{U}_{ij}^n = \frac{1}{\Delta x_i^1 \, \Delta x_j^2} \int_{x_{j-1/2}^2}^{x_{j+1/2}^2} \int_{x_{i-1/2}^1}^{x_{i+1/2}^1} P_{ij}^n(x^1, x^2)\, dx^1 dx^2, \tag{12}$$

where $\overline{U}_{ij}^n$ is the cell-average at time $t = t^n$. The reconstruction polynomials can be obtained by different approaches, in the present context, we employ high-order WENO scheme, briefly outlined below, the details are described in [31], The scheme considered herein is non-oscillatory and is capable of removing the oscillations, but there is no guarantee that it would keep the numerical solution within the physical bounds, this issue may occur near the flux evaluation step. To ensure the numerical solution is always between the physical bounds, which is a basic requirement of atmospheric models we have coupled a bound preserving filter with the CUFV scheme. The details of the filter are mentioned in [38].

### 3.1. Dimension-split fifth-order WENO reconstructions

WENO methods are deemed to be robust for solving conservation laws, Shu in his work [39], has given inclusive assessment of WENO schemes. We consider CUFV scheme based on WENO reconstruction method, where fifth-order accurate 1D reconstruction is used in a dimension-split (i.e. dimension-by-dimension) manner, hereafter this is referred to as WENO-5. The WENO-5 scheme is widely used for various applications, including atmospheric modeling [31,40], Bryson and Levy [37] utilized a 1D central WENO-5 scheme for a system of conservation laws. The reconstruction polynomial $P_{ij}^n(x^1, x^2)$ is based on 1D WENO-5 scheme, and used in a dimension-by-dimension manner which splits the 2D scheme into two 1D reconstructions along each coordinate direction (i.e., $x^1$ and $x^2$ directions).

Fig. 2 shows the computational stencil used for CUFV schemes. The thick solid lines portrayed in Fig. 2 represent the computational stencil (five cell-wide in each direction) for WENO-5 scheme. For a single cell $\Omega_{ij}$ as shown in Fig. 2 (right panel), two 1D WENO-5 polynomials are constructed along W-E and S-N directions, for estimating four point-values on the cell edges at east, north, west and south sides. These are shown in Fig. 2 (right panel) as E, N, W and S, respectively. Thus, flux evaluation for the split-scheme requires only at four points on cell walls, in this case flux integral (10) simplifies into a point-value estimation. The dimension-split approach makes the computational procedure relatively simple, particularly on cubed-sphere grid where the corner ghost cells are not required [31]. The WENO-5 implementation on the cubed-sphere closely follows that described in Katta et al. [31], therefore we skip the details herein.

### 3.2. Special treatment for cubed-sphere edges

Cubed-sphere is essentially a patched domain consists of subdomains (faces) with discontinuous edges and corners as shown in Fig. 1. This necessitates special treatment for the high-order FV scheme which requires wider halo region. WENO-5

reconstruction scheme requires a halo region spanning at least two cells from either side of the neighboring panels. Because of the dimension-split approach WENO-5 does not require corner cells. Recently, Katta et al. [31] have implemented CUFV schemes for linear transport problems on the cubed-sphere by extending the grid-lines by two grid cells at the edges. Note that the cubed-sphere grid-lines $(x^1, x^2)$ are great-circle arcs [33], the cells can be extended beyond its usual range $[\pi/4, -\pi/4]$ by means of high order 1D interpolation. We use this strategy, where 1D interpolations performed along the great-circle arcs as indicated in Fig. 1 right panel.The treatment of edges is discussed in detail in [31], so the details are not mentioned herein.

The covariant velocity vectors $(u_1, u_2)$, i.e., prognostic variables in the momentum equations, are not in general continuous across the cubed-sphere edges due to the inherent coordinate discontinuity at the cubed-sphere edges. To make the reconstruction process smooth, we consider the orthogonal spherical velocity components $(u_s, v_s)$ which are smooth over the entire domain. The velocity fields $(u_1, u_2)$ can be easily converted to $(u_s, v_s)$ through the transformation (2). The derivative quantity such as vorticity filed $(\zeta)$ is computed using a high-order central differencing method. At the edges, we employ backward or forward differencing method (one-sided) depending on the location as discussed in [17]. Note that because of the equiangular central projection considered for the cubed-sphere geometry, $\Delta x_i^1 = \Delta x_j^2$, which simplifies the computation.

### 3.3. Time integration scheme (SSP-RK3 scheme)

The semi-discretized ODE represented in Eq. (9) should be solved to attain the solution in next time step, this semi-discrete FV scheme can be represented in the following general form:

$$\frac{d}{dt}\bar{U}(t) = L(\bar{U}) \qquad \text{in } (0, T]. \tag{13}$$

There are a wide variety of time integrators available to solve the ODE (13), however, we consider the explicit Runge–Kutta (RK) time integration methods.

In the present work, we use a strong stability preserving (SSP) third-order and three-stage RK (SSP-RK3) time integration [41] for the proposed FV schemes. The SSP time integration schemes are widely used in DG literature [42], the advantages of this type of time integration scheme include: they do not generate new local maxima or minima (or total variation diminishing property in time) due to the time discretization. The SSP-RK3 scheme can be represented as follows,

$$\bar{U}^{(1)} = \left[\bar{U}^n + \Delta t L(\bar{U}^n)\right],$$

$$\bar{U}^{(2)} = \frac{3}{4}\bar{U}^n + \frac{1}{4}\left[\bar{U}^{(1)} + \Delta t L(\bar{U}^{(1)})\right],$$

$$\bar{U}^{n+1} = \frac{1}{3}\bar{U}^n + \frac{2}{3}\left[\bar{U}^{(2)} + \Delta t L(\bar{U}^{(2)})\right].$$

where the superscripts $n$ and $n+1$ denote time levels $t$ and $t + \Delta t$, respectively. The CFL limit for FV scheme with SSP-RK3 is approximately 1.00.

## 4. Numerical experiments and results

Williamson et al. [16] proposed a suite of benchmark test cases for SW equations on the sphere. We consider 3 tests from the suite, which are widely used for validating SW models. For better consistency, the initial data for the test is computed from $3 \times 3$ point-values (see the right stencil shown in Fig. 2) on each FV cell. The cell-averaged value $\overline{U}_{ij}$ for the scheme is computed using the following formula based on Simpsons rule:

$$\overline{U}_{ij} = \frac{1}{36}\Big(U_{i-1/2,j-1/2} + U_{i-1/2,j+1/2} + U_{i+1/2,j-1/2} + U_{i+1/2,j+1/2} + 4U_{i-1/2,j} + 4U_{i+1/2,j} + 4U_{i,j-1/2} + 4U_{i,j+1/2} + 16U_{ij}\Big). \tag{14}$$

The normalized standard errors $L_1$, $L_2$ and $L_\infty$ [16], are used for comparing WENO-5 and KL schemes for one of the test cases where the analytic solution is known.

### 4.1. Steady state geostropic flow

The first test considered is a steady-state geostropic flow test problem, which has a steady-state solution of the full non-linear SW equations. The wind field is uniform and the equations are geostropically balanced during the time evolution. So, both the height and flow fields remain same during the simulation. For this particular test analytical solution is the same as initial condition. The initial velocity and height fields can be given as follows:

$$u = u_0(\cos\alpha_0 \cos\theta + \sin\alpha_0 \cos\lambda \sin\theta)$$

$$v = -u_0 \sin\alpha_0 \sin\lambda$$

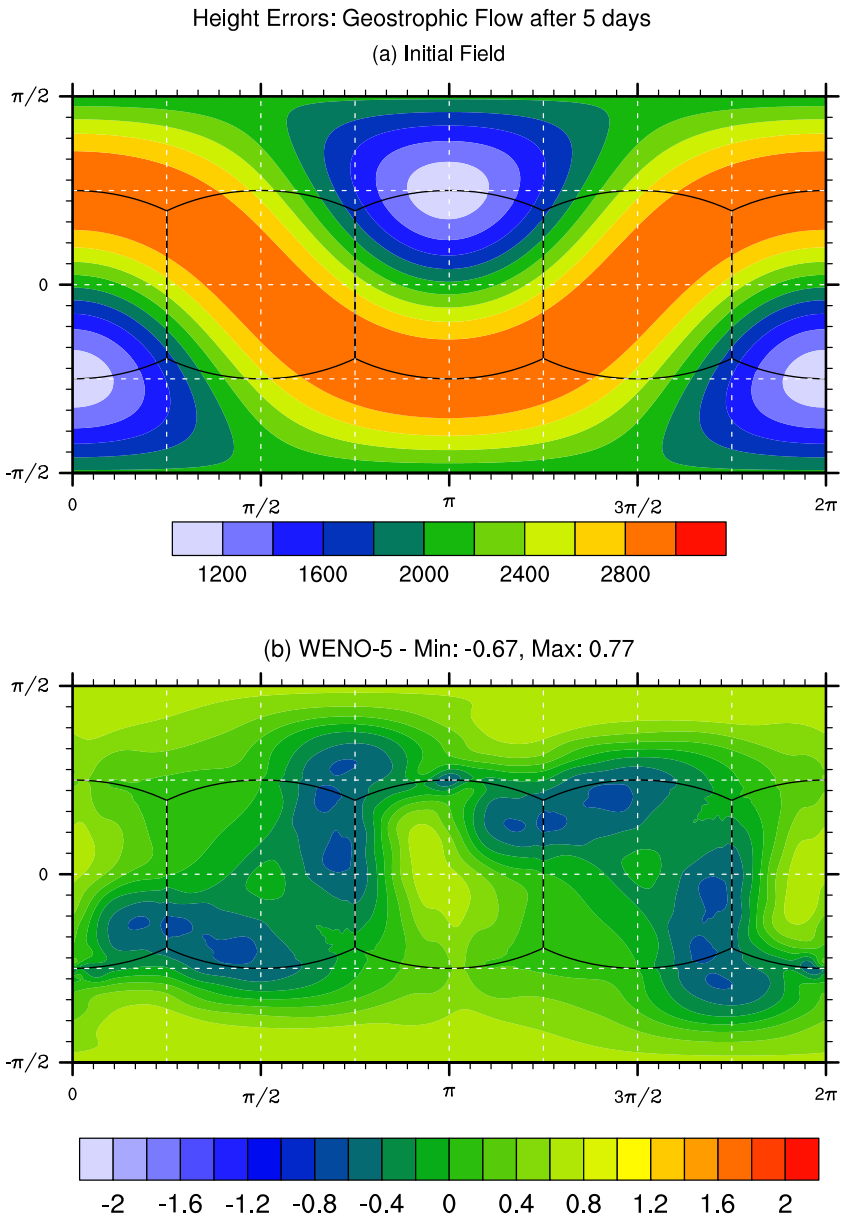


**Fig. 3.** Height errors (numerical − analytic) after 5 days with steady state geostrophic flow test on $40 \times 40 \times 6$ grid, and a CFL of 0.50 is chosen. (a) Initial height field and (b) WENO-5. Contour lines for (b) are plotted from −2.0 to 2.0 with an interval of 0.2 m.

$$gh = gh_0 - \frac{u_0}{2}(2a\omega + u_0)(\sin\theta\cos\alpha_0 - \cos\lambda\cos\theta\sin\alpha_0)^2$$

where $a$ is the earth's radius, $u_0 = 2\pi a/(12 \text{ days})$ and $gh_0 = 2.94 \times 10^4 \text{m}^2\ \text{s}^{-2}$. Here we chose alpha $\alpha_0 = \pi/4$, which makes the test more challenging on the cubed-sphere. The numerical results of height (error = numerical − analytic) and vorticity fields after 5 model days are given in Fig. 3 for WENO-5 scheme. The grid resolution considered is $40 \times 40 \times 6$ and a CFL limit of 0.50 is chosen for this test case. The normalized $L_1$, $L_2$ and $L_\infty$ errors for WENO-5 are 1.41E–4 , 1.59E–4 and 2.58E–4 respectively. As compared to results with other high-order SW models [3,17,18], the absolute error plots seems to be smooth, and this may due to the diffusive nature of the flux scheme (11) used for the CUFV scheme.

### *4.2. Zonal flow over an isolated mountain*

The second test we considered is listed as the SW test-case 5 in [16], which consists of a zonal flow of a shallow fluid over an isolated mountain. The wind and height fields are the same as in the previous test, except for the parameters $\alpha_0 = 0$, $h_0 = 5960$ m

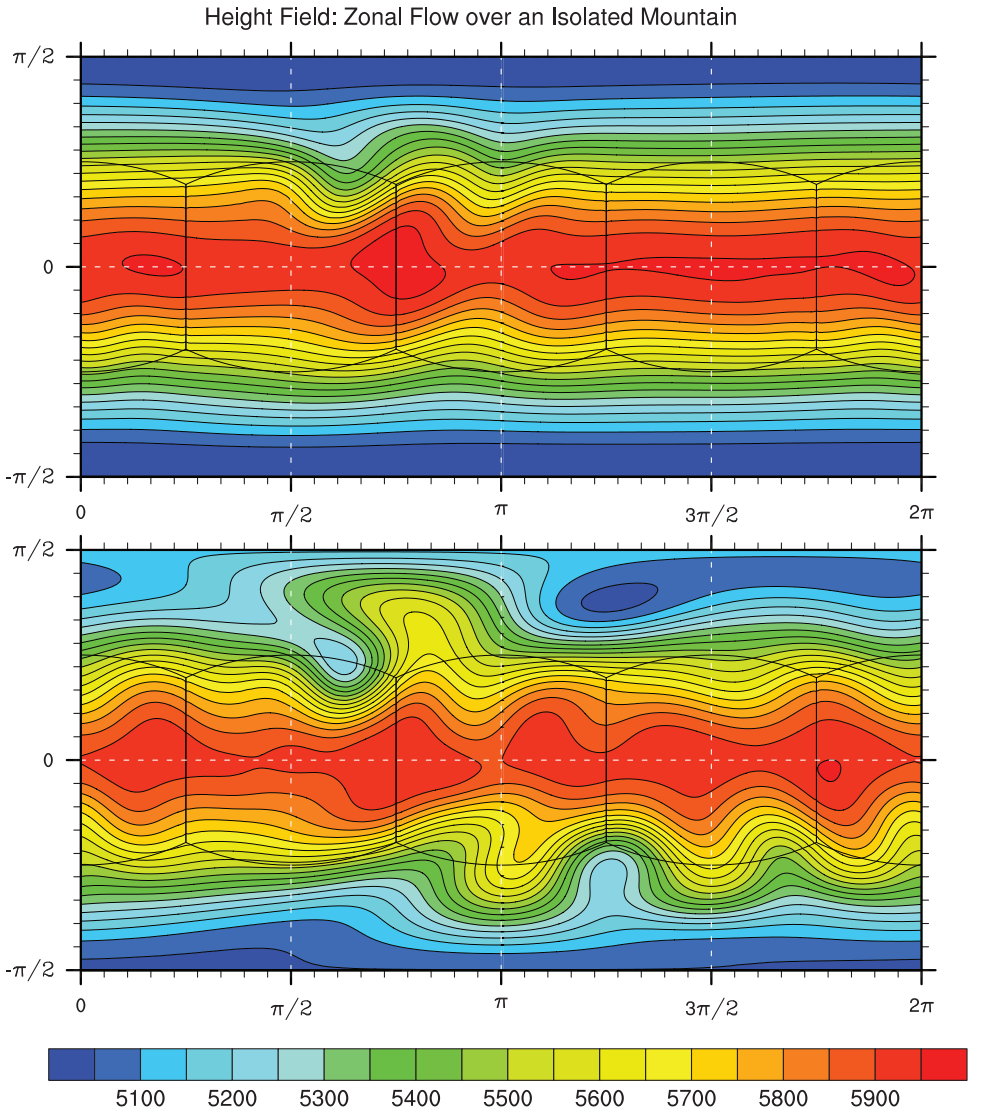


**Fig. 4.** Numerical solution for the zonal flow over an isolated mountain test on $40 \times 40 \times 6$ grid and CFL = 0.50. Contour levels are from 5050 m to 5950 m in intervals of 50 m. The top and bottom rows represent the solution obtained by WENO-5 scheme at 5 and 15 days respectively.

and $u_0 = 20$ m/s . The bottom of the "mountain" is centered at $(\lambda_c, \theta_c) = (3\pi/2, \pi/6)$, and defined by the following:

$$h_s = h_{s0}\left(1 - r/r_0\right),$$

where $h_{s0} = 2000$ m, $r_0 = \pi/9$ and $r = \min\left[r_0, \sqrt{(\lambda - \lambda_c)^2 + (\theta - \theta_c)^2}\right]$.

There is no analytic solution available to this test case, we compare the results of the solution with other high-order FV results in literature. The Numerical solution of height field and vorticity field is shown in Figs. 4 and 5 respectively. The simulation is carried out on $40 \times 40 \times 6$ grid, and CFL = 0.50 is chosen. The results with high-order multi moment FV model [18] and a fourth-order upwind FV model [17] shows comparable results for this test. The evolution of vorticity fields across the cubed-sphere edges found to be smooth (Fig. 5). Time traces of normalized errors of potential enstrophy and total energy are given in Fig. 6, and the errors are comparable to the results given in [17]; conservation of mass ($h$) is up to the machine-precision and therefore not shown here.

### 4.3. Rossby–Haurwitz wave

A 4-wave Rossby–Haurwitz wave (test case 6 in [16]) is considered as the third experiment in this present work. The initial state is an exact steadily propagating solution of the non-divergent barotropic vorticity equation. This case is not considered for

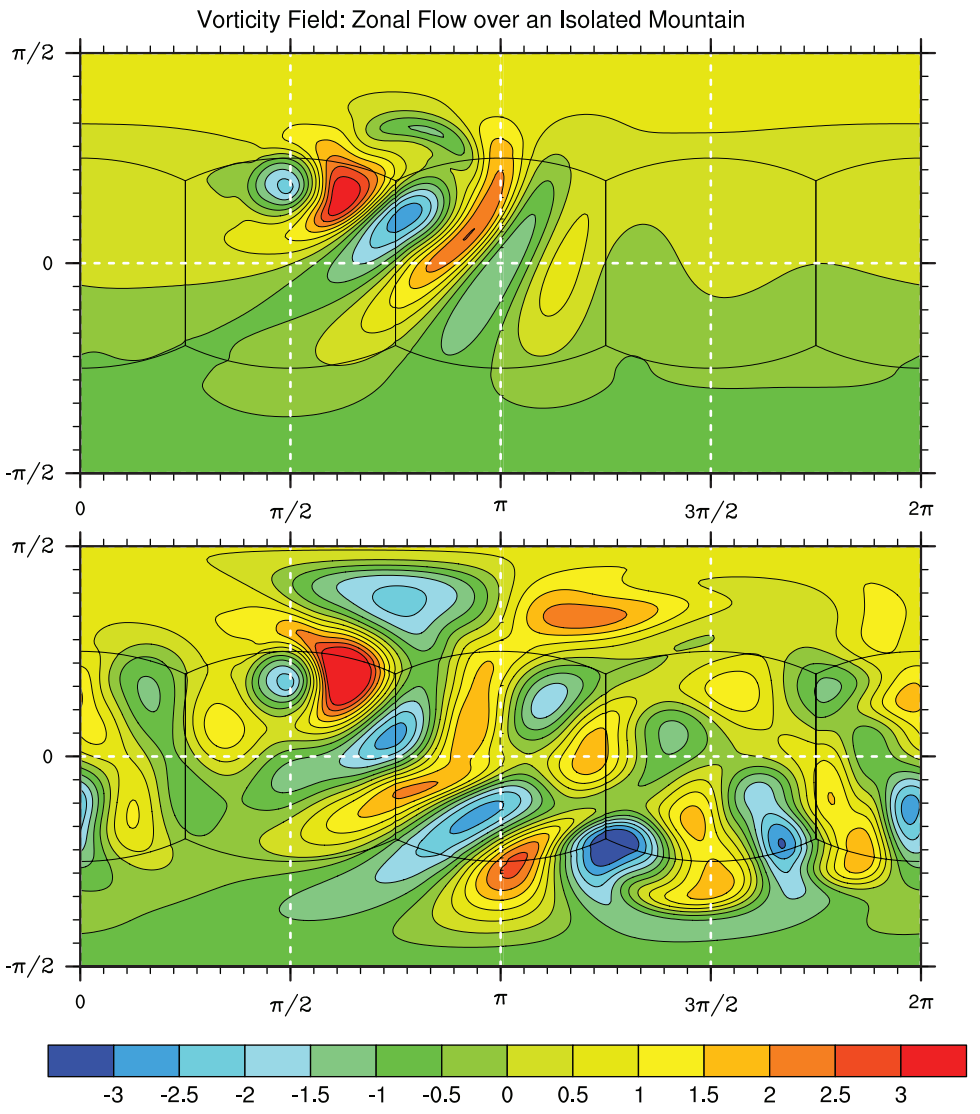


**Fig. 5.** Numerical solution of vorticity field ($\zeta$) for the zonal flow over an isolated mountain test, experiment settings are same as in Fig. 4. Contour levels are from ($-3$ to 3 in intervals of .50) $\times$ $10^{-5}$ $s^{-1}$. The top and bottom rows represent the solution obtained by WENO-5 scheme at 5 and 15 days respectively.

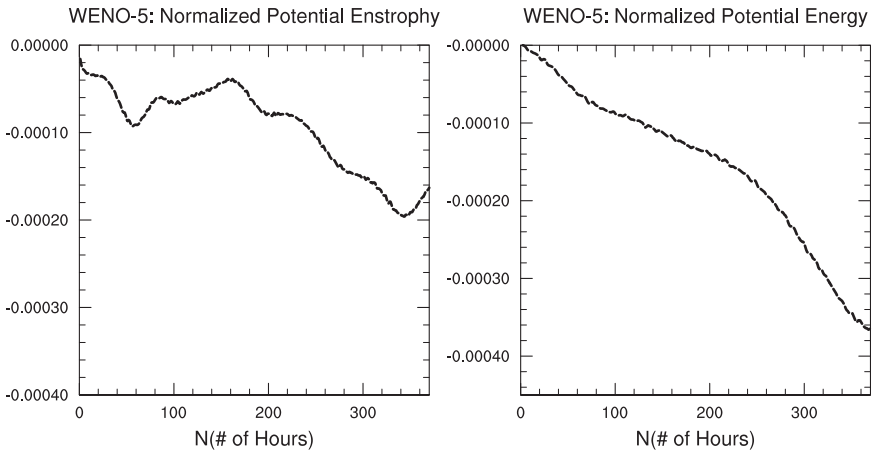


**Fig. 6.** All the experiment settings are same as in Fig. 4. Evolution of the normalized errors of potential enstrophy (left) and total energy (right).

testing the long-term performance of a numerical model, because it is dynamically instable, but it still provides a good test bed for short to middle-term simulations. The divergence-free flow field can be given by the following:

$$\psi = -R^2\omega \sin\theta + R^2 K \cos^2\theta \sin\theta \cos r\lambda$$

the initial field is given by:

$$gh = gh_0 + R^2 A + R^2 B \cos r\lambda + R^2 C \cos 2r\lambda$$

Here $\omega = K = 7.848 \times 10^{-6} s^{-1}$ and $r = 4$ are the constants, and A, B, and C are the functions of latitude. Please refer to [16] for complete details for this test case. The Numerical solution of height field is shown in Fig. 7. The simulation is carried out on $48 \times 48 \times 6$ grid, and CFL = 0.50 is chosen. From the comparison to other results given in literature we found that WENO-5 scheme produces accurate results. The evolution of normalized errors of potential enstrophy and total energy are given in Fig. 8, the errors are comparable to the results reported with the high-order FV model [17]. In order to be consistent with the test-case 5, we chose a resolution of $40 \times 40 \times 6$ to produce the normalized errors.

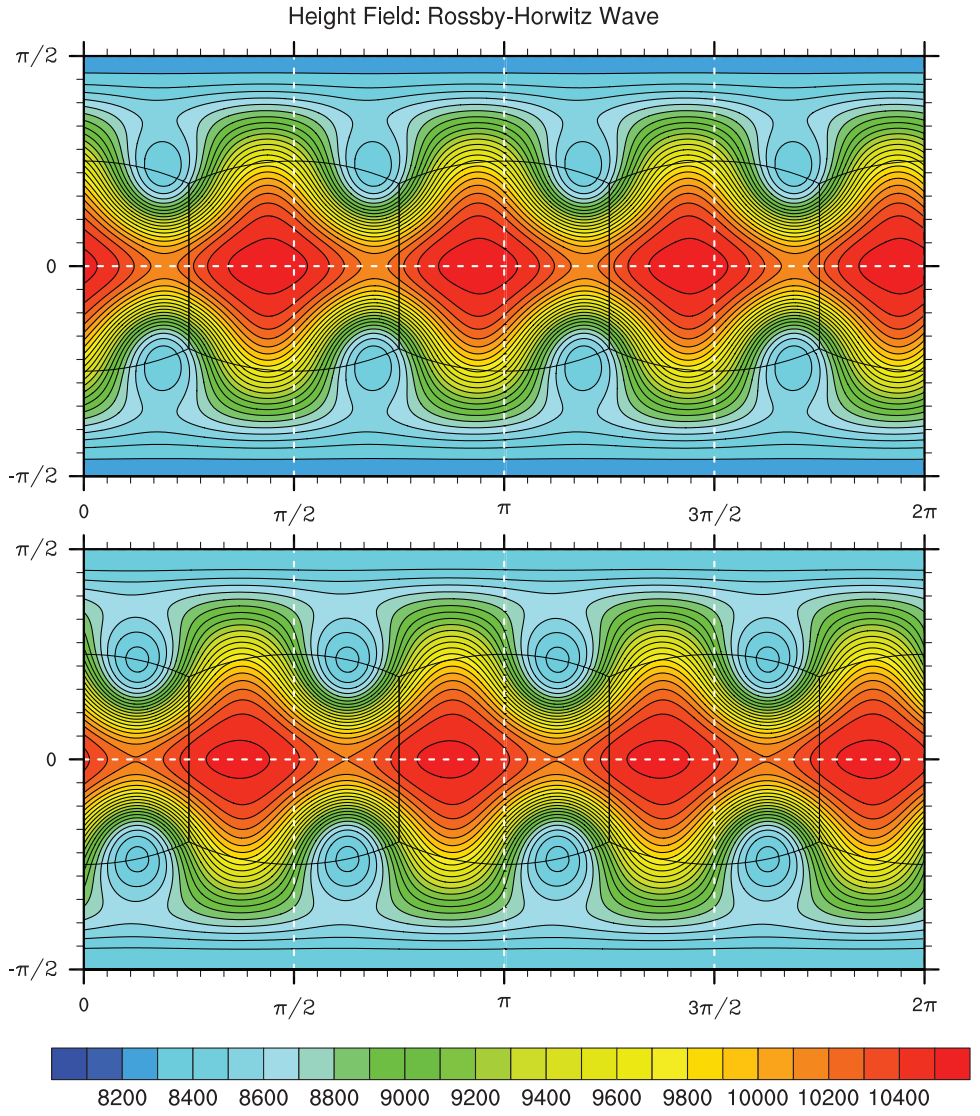


**Fig. 7.** Numerical solution for the Rossby–Haurwitz wave test on $48 \times 48 \times 6$ grid and CFL = 0.50. Contour levels are from 8100 m to 10,500 m in intervals of 100 m. The top and bottom rows represents the solution obtained by WENO-5 scheme, the left and right columns represents the solution at 7 and 14 days respectively.

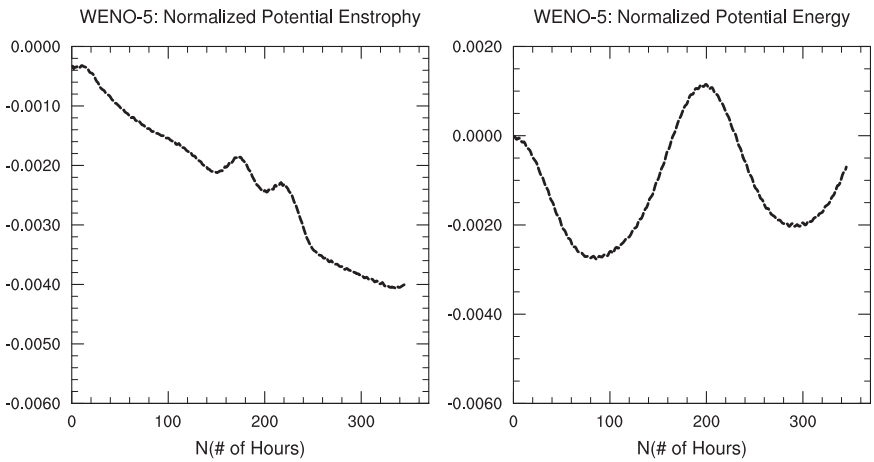


**Fig. 8.** All the experiment settings are same as in Fig. 7, except the grid resolution is $40 \times 40 \times 6$. Evolution of the normalized conservation errors of potential enstrophy (left) and total energy (right).

## 5. Summary and conclusions

The central-upwind finite-volume (CUFV) scheme developed for linear transport problem by Katta et al. [31] have been extended for the shallow-water equations on the cubed-sphere. We consider semi-discretized high-order CUFV scheme with a dimension-split fifth-order WENO reconstruction (WENO-5). The flux computations are based on flux formula introduced in Kurganov et al. [24,25], a compact approach which relies on one-sided local speed. Time integration is performed with a third-order Runge–Kutta method, and several standard benchmark tests have been considered to validate the CUFV based SW model.

A novel feature of this method is its simplicity, in terms of implementation. The CUFV scheme does not rely on characteristic decomposition or expensive Riemann solvers, moreover, a staggered grid [14] is not required. This feature greatly simplifies implementation in complex domain such as the cubed-sphere. The high-order dimension-split approach on the cubed-sphere did not create any significant accuracy issue as compared to a fourth-order fully 2D reconstruction, which is consistent with the results reported for liner transport problems in Katta et al. [31]. The nonlinear shallow-water results are comparable to those with high-order conventional upwind based Godunov-type FV SW models [17,18]. The fourth-order FV scheme [17] requires a sophisticated Riemann solver combined with an ortho-normalization procedure for the SW model on nonorthogonal curvilinear cubed-sphere domain, however, CUFV SW model does not require any of these to produce comparable results as demonstrated for the unsteady test cases. For the steady steady-state case, CUFV SW model results seems to be more diffusive as compared to upwind based models [17,18], a less diffusive flux formula might improve this deficiency.

High-order WENO reconstructions schemes are expensive as opposed to regular polynomial reconstructions, in a fully 2D (unsplit) case they are computationally prohibitive for practical application. In our experience with CUFV SW model, the results with dimension-split WENO-5 scheme is comparable to that with the Kurganov–Liu (KL) scheme (results of KL scheme are not reported here, since they are identical to that of the results obtained by WENO-5 scheme) in terms of quality and computational expense, this corroborates the results reported in [31] for linear problems. The foremost disadvantage of WENO-5 scheme is the reduction in the formal order of accuracy of the resulting 2D scheme due to the dimension-split approach even though the 1D component of WENO5 scheme is fifth-order accurate. However, for cubed-sphere implementation WENO-5 is more preferable because of the simple stencil (there is no need for corner ghost cells). The 1D method used for creating halo regions in the present work might not be the most accurate and efficient solution, especially for high-order FV scheme. We would further investigate the possibility of employing halo regions using 2D interpolations for future extension. The 2D CUFV schemes considered herein will be further tested to a 3D non-hydrostatic atmospheric model in future.

## Acknowledgments

First author wish to acknowledge Dr. Richard Loft for the SIParCS internship at IMAGe, and Dr. Christopher Davis for the ASP graduate student visit opportunity for accomplishing this work at NCAR. Many thanks to Evan Bollig, for helpful discussions. Finally Katta is thankful to Dr. Leticia Velazquez, Director of CPS Program at UTEP, for the financial support provided during his doctoral studies. R.D.N. is thankful to the US DOE BER #DE-SC0001658 support.

## References

[1] M. Taylor, J. Tribbia, M. Iskandarani, The spectral element method for the shallow water equations on the sphere, J. Comput. Phys. 130 (1997) 92–108.
[2] F.X. Giraldo, Lagrange-Galerkin methods on spherical geodesic grids: the shallow water equations, J. Comput. Phys. 160 (2000) 336–368.

[3] R.D. Nair, S.J. Thomas, R.D. Loft, A discontinuous Galerkin global shallow water model, Mon. Wea. Rev. 133 (2005) 876–888.
[4] M.K. Kadalbajoo, V. Gupta, A brief survey on numerical methods for solving singularly perturbed problems, Appl. Math. Comput. 217 (8) (2010) 3641–3716. doi: http://dx.doi.org/10.1016/j.amc.2010.09.059. URL http://www.sciencedirect.com/science/article/pii/S0096300310010532.
[5] P. Rao, Numerical modeling of open channel flows using a multiple grid {ENO} scheme, Appl. Math. Comput. 161 (2) (2005) 599–610. doi: http://dx.doi.org/10.1016/j.amc.2003.12.051. URL http://www.sciencedirect.com/science/article/pii/S0096300304000141.
[6] F. Rus, F.R. Villatoro, Time-stepping in Petrov–Galerkin methods based on cubic b-splines for compactons, Appl. Math. Comput. 217 (6) (2010) 2788–2797. doi: http://dx.doi.org/10.1016/j.amc.2010.08.013. URL http://www.sciencedirect.com/science/article/pii/S0096300310008672.
[7] S. Saker, Oscillation of parabolic neutral delay difference equations with several positive and negative coefficients, Appl. Math. Comput. 143 (1) (2003) 173–186. doi: http://dx.doi.org/10.1016/S0096-3003(02)00366-1. URL http://www.sciencedirect.com/science/article/pii/S0096300302003661.
[8] J. Thuburn, A PV-based shallow-water model on a hexagonal-icosahedral grid, Mon. Wea. Rev. 125 (1997) 2328–2350.
[9] D. Majewski, D. Liermann, P. Prohl, B. Ritter, M. Buchhold, T. Hanisch, G. Paul, W. Wergen, J. Baumgardner, The operational global icosahedral-hexagonal gridpoint model GME: Description and high-resolution tests, Mon. Wea. Rev. 130 (2002) 319–338.
[10] H. Tomita, M. Tsugawa, M. Satoh, K. Goto, Shallow water model on a modified icosahedral geodesic grid using spring dynamics, J. Comput. Phys. 174 (2001) 579–613.
[11] X. Peng, F. Xiao, K. Takahashi, Conservative constraint for a quasi-uniform overset grid on the sphere, Quart. J. Roy. Meteor. Soc. 132 (2006) 979–996.
[12] R. Sadourny, Conservative finite-difference approximations of the primitive equations on quasi-uniform spherical grids, Mon. Wea. Rev. 100 (1972) 136–144.
[13] M. Rančić, R. Purser, F. Mesinger, A global shallow water model using an expanded spherical cube, Q. J. R. Meteorol. Soc. 122 (1996) 959–982.
[14] W.M. Putman, S.J. Lin, A finite-volume dynamical core on the cubed-sphere grid, in: Numerical Modeling of Space Plasma Flows: ASTRONUM-2008, in: Astronomical Society of the Pacific Conference Series, 406, 2009, pp. 268–275.
[15] C. Yang, X. Cai, Parallel multilevel methods for implicit solution of shallow water equations with nonsmooth topography on the cubed-sphere, J. Comput. Phys. 230 (2011) 2523–2539.
[16] D.L. Williamson, J.B. Drake, J.J. Hack, R. Jakob, P.N. Swarztrauber, A standard test set for numerical approximations to the shallow water equations in spherical geometry, J. Comput. Phys. 102 (1992) 211–224.
[17] P.A. Ullrich, C. Jablonowski, B. van Leer, High-order finite-volume methods for the shallow-water equations on the sphere, J. Comput. Phys. 229 (2010) 6104–6134.
[18] C. Chen, F. Xiao, Shallow water model on cubed-sphere by multi-moment finite volume method, J. Comput. Phys. 227 (2008) 5019–5044.
[19] J. Escobar-Vargas, P. Diamessis, F. Giraldo, High-order discontinuous element-based schemes for the inviscid shallow water equations: Spectral multidomain penalty and discontinuous Galerkin methods, Appl. Math. Comput. 218 (9) (2012) 4825–4848. doi: http://dx.doi.org/10.1016/j.amc.2011.10.046. URL http://www.sciencedirect.com/science/article/pii/S0096300311012914.
[20] E.F. Toro, Riemann Solvers and Numerical Methods for Fluid Dynamics. A Practical Introduction, 2nd ed., Springer-Verlag, New York, 1999.
[21] N. Crnjaric-Zic, B. Crnkovic, High order accurate semi-implicit {WENO} schemes for hyperbolic balance laws, Appl. Math. Comput. 217 (21) (2011) 8611–8629. doi: http://dx.doi.org/10.1016/j.amc.2011.03.098. URL http://www.sciencedirect.com/science/article/pii/S0096300311004668.
[22] D. liang Qiao, P. Zhang, S. Wong, K. Choi, Discontinuous Galerkin finite element scheme for a conserved higher-order traffic flow model by exploring Riemann solvers, Appl. Math. Comput. 244 (0) (2014) 567–576. doi: http://dx.doi.org/10.1016/j.amc.2014.07.002. URL http://www.sciencedirect.com/science/article/pii/S009630031400959X.
[23] H. Nessyahu, E. Tadmor, Nonoscillatory central differencing for hyperbolic conservation laws, J. Comput. Phys. 87 (1990) 408–463.
[24] A. Kurganov, G. Petrova, A third-order semi-discrete genuinely multidimensional central scheme for hyperbolic conservation laws and related problems, Numer. Math. 88 (2001) 683–729.
[25] A. Kurganov, S. Noelle, G. Petrova, Semi-discrete central-upwind schemes for hyperbolic conservation laws and Hamilton–Jacobi equations, SIAM J. Sci. Comput. 23 (2000) 707–740.
[26] D. Levy, G. Puppo, G. Russo, Compact central weno schemes for multidimensional conservation laws, SIAM J. Sci. Comput. 22 (2000) 656–672.
[27] L. Tang, Upwind and central {WENO} schemes, Appl. Math. Comput. 166 (2) (2005) 434–448. doi: http://dx.doi.org/10.1016/j.amc.2004.06.043. URL http://www.sciencedirect.com/science/article/pii/S0096300304004485.
[28] H. Feng, C. Huang, R. Wang, An improved mapped weighted essentially non-oscillatory scheme, Appl. Math. Comput. 232 (0) (2014) 453–468.doi: http://dx.doi.org/10.1016/j.amc.2014.01.061. URL http://www.sciencedirect.com/science/article/pii/S0096300314000988.
[29] X. Liu, S. Osher, T. Chen, Weighted essentially non-oscillatory schemes, J. Comput. Phys. 115 (1994) 200–212.
[30] G.S. Jiang, C.W. Shu, Efficient implementation of weighted ENO schemes, J. Comput. Phys. 126 (1996) 202–228.
[31] K.K. Katta, R.D. Nair, V. Kumar, High-order finite volume transport on the cubed-sphere: comparison between 1D and 2D reconstruction schemes, Mon. Wea. Rev. (2014). URL http://dx.doi.org/10.1175/MWR-D-13-00176.1.
[32] R.D. Nair, K.K. Katta, The central-upwind finite-volume method for atmospheric numerical modeling, Contemp. Math. 586 (2013) 277–285.
[33] C. Ronchi, R. Iacono, P.S. Paolucci, The "cubed sphere": a new method for the solution of partial differential equations in spherical geometry, J. Comput. Phys. 124 (1) (1996) 93–114.
[34] S. Adjerid, P. Moore, J.D. Teresco, Preface, Appl. Numerical Math. 52 (23) (2005) 129–132 doi: http://dx.doi.org/10.1016/j.apnum.2004.08.042. URL http://www.sciencedirect.com/science/article/pii/S0168927404001618. {ADAPT} '03: Conference on Adaptive Methods for Partial Differential Equations and Large-Scale Computation
[35] R.D. Nair, S.J. Thomas, R.D. Loft, A discontinuous Galerkin transport scheme on the cubed-sphere, Mon. Wea. Rev. 133 (2005) 814–828.
[36] L. Bao, R.D. Nair, H. Tufo, A mass and momentum flux-form high-order discontinuous Galerkin shallow water model on the cubed-sphere, J. Comput. Phys. (2013).
[37] S. Bryson, D. Levy, On the total variation of high-order semi-discrete central schemes for conservation laws, J. Sci. Comput. 22 (2006) 163–175.
[38] Y. Zhang, R.D.N. Nair, A nonoscillatory discontinuous Galerkin transport scheme on the cubed sphere, Mon. Wea. Rev. 140 (9) (2012) 3106–3126. URL http://dx.doi.org/10.1175/MWR-D-11-00287.1.
[39] C.-W. Shu, Essentially non-oscillatory and weighed essentially non-oscillatory schemes for hyperbolic conservation laws, in: Lecture Notes in Mathematics, 1697, Springer, 1997, pp. 325–432.
[40] M.R. Norman, R.D. Nair, F.H.M. Semazzi, A low communication and large time step explicit finite-volume solver for non-hydrostatic atmospheric dynamics, J. Comput. Phys. 230 (2011) 1567–1584.
[41] S. Gottlieb, C.W. Shu, E. Tadmor, Strong stability preserving high-order time discretization methods, SIAM Rev. 43 (2001) 89–112.
[42] B. Cockburn, C.-W. Shu, The local discontinuous Galerkin for convection diffusion systems, SIAM J. Numer. Anal. 35 (1998) 2440–2463.